

1 **Magnetic anisotropy in natural amphibole crystals**

2

3 Andrea R. Biedermann^{1,a}, Christian Bender Koch², Thomas Pettke³ and Ann M. Hirt^{1,*}

4 ¹ Institute of Geophysics, ETH Zurich, Sonneggstrasse 5, 8092 Zurich, Switzerland;

5 ^a Now at Department of Geology and Mineral Resources Engineering, Norwegian University
6 of Science and Technology, Sem Sælands vei 1, 7491 Trondheim, Norway

7 ² Department of Chemistry, University of Copenhagen, Universitetsparken 5, 2100
8 Copenhagen Ø, Denmark;

9 ³ Institute of Geological Sciences, University of Bern, Baltzerstrasse 1-3, 3012 Bern,
10 Switzerland;

11

12 The final version of this article is available from the American Mineralogist website, doi:
13 10.2138/am-2015-5173

14

15 <http://ammin.geoscienceworld.org/content/100/8-9/1940>

16

17

18 **Keywords:** AMS (Anisotropy of magnetic susceptibility), magnetic properties, single crystal,
19 amphibole, hornblende, actinolite, richterite, tremolite

20

21 **Abstract**

22 Anisotropy of magnetic susceptibility (AMS) is often used as a proxy for mineral
23 fabric in deformed rocks. In order to do so quantitatively, it is necessary to quantify the
24 intrinsic magnetic anisotropy of single crystals of rock-forming minerals. Amphiboles are
25 common in mafic igneous and metamorphic rocks and often define rock texture due to their
26 general prismatic crystal habits. Amphiboles may dominate the magnetic anisotropy in
27 intermediate to felsic igneous rocks and in some metamorphic rock types, because they have a
28 high Fe concentration and they can develop a strong crystallographic preferred orientation. In
29 this study, the AMS is characterized in 28 single crystals and one crystal aggregate of
30 compositionally diverse clino- and ortho-amphiboles. High-field methods were used to isolate
31 the paramagnetic component of the anisotropy, which is unaffected by ferromagnetic
32 inclusions that often occur in amphibole crystals. Laue imaging, laser ablation inductively
33 coupled plasma mass spectrometry and Mössbauer spectroscopy were performed to relate the
34 magnetic anisotropy to crystal structure and Fe concentration. The minimum susceptibility is
35 parallel to the crystallographic a^* -axis and the maximum susceptibility is generally parallel to
36 the crystallographic b -axis in tremolite, actinolite, and hornblende. Gedrite has its minimum
37 susceptibility along the a -axis, and maximum susceptibility aligned with c . In richterite,
38 however, the intermediate susceptibility is parallel to the b -axis and the minimum and
39 maximum susceptibility directions are distributed in the a - c -plane. The degree of anisotropy,
40 k' , increases generally with Fe concentration, following a linear trend described by: $k' =$
41 $1.61 \times 10^{-9} \text{ Fe} - 1.17 \times 10^{-9} \text{ m}^3/\text{kg}$. Additionally, it may depend on the $\text{Fe}^{2+}/\text{Fe}^{3+}$ ratio. For most
42 samples, the degree of anisotropy increases by a factor of approximately 8 upon cooling from
43 room temperature to 77 K. Ferroactinolite, one pargasite crystal and riebeckite show a larger
44 increase, which is related to the onset of local ferromagnetic (*s.l.*) interactions below about
45 100 K. This comprehensive data set increases our understanding of the magnetic structure of
46 amphiboles, and it is central to interpreting magnetic fabrics of rocks whose AMS is
47 controlled by amphibole minerals.

48

49 **1. Introduction**

50 Members of the amphibole group are common rock forming minerals occurring in a
51 wide range of igneous and metamorphic rocks. Amphiboles crystallize generally in
52 idiomorphic, prismatic to needle-like habits; hence they often display preferential orientation

53 in a deformed rock. This, combined with their intrinsic magnetic anisotropy, often makes
54 amphiboles, together with phyllosilicates, the main carriers of magnetic anisotropy in igneous
55 and metamorphic rocks. Amphiboles can be responsible for the magnetic fabric of a rock in
56 two ways. Firstly, the amphibole minerals themselves can dominate the paramagnetic
57 anisotropy (e.g. Borradaile et al. 1993; Schulmann and Ježek 2011; Zak et al. 2008).
58 Secondly, the shape of magnetite inclusions can be controlled by the crystallographic
59 preferred orientation (CPO) of amphiboles, which in turn is responsible for the magnetic
60 anisotropy (Archanjo et al. 1994).

61 Because amphiboles possessing a CPO can be an important carrier of the magnetic
62 anisotropy in a rock, it is essential to quantify their intrinsic anisotropy of magnetic
63 susceptibility (AMS). Until now, only a few studies have been conducted on the AMS of
64 amphibole single crystals, returning inconsistent results. Finke (1909) measured one
65 hornblende crystal and found the maximum susceptibility at an angle of $-21^{\circ}55'$ to the
66 crystallographic *c*-axis. Wagner et al. (1981) measured the magnetic anisotropy in six crystals
67 from the hornblende group. In addition, they cited an unpublished study by Parry (1971), who
68 examined high-field AMS in 18 hornblende crystals. Both studies concluded that the
69 maximum principal susceptibility is sub-parallel to the crystallographic *c*-axis. However, in
70 Wagner's hornblende, the minimum susceptibility aligns with the crystallographic *a*-axis,
71 whereas it is parallel to *b* in Parry's study. This difference was attributed to the presence of
72 ferromagnetic inclusions that influenced Wagner's low-field measurements (Wagner et al.
73 1981). Borradaile et al. (1987) measured five aggregates of amphibole crystals, including two
74 actinolites and one sample each of hornblende, crocidolite (fibrous riebeckite) and
75 glaucophane. Due to imperfect alignment of the individual grains within the aggregates, this
76 study gives an estimate of the lower limit of the AMS. The authors provide no directional

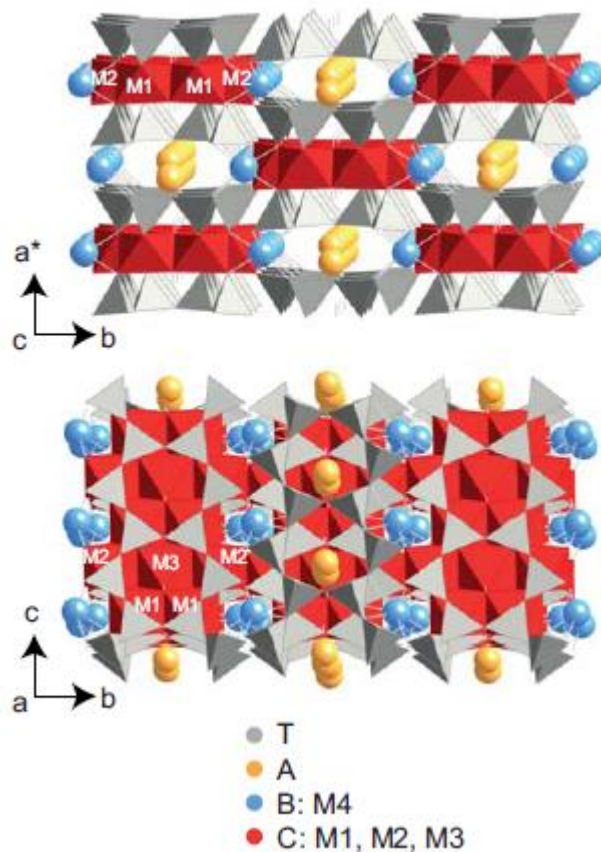
77 dependency. Lagroix and Borradaile (2000) measured two pargasite crystals and suggested
78 that the maximum susceptibility is sub-parallel to the *b*-axis.

79 Differences in orientations of the principal axes of the AMS ellipsoid reported in these
80 previous studies illustrate the importance of systematically investigating the magnetic
81 anisotropy of amphiboles. In the present study, the intrinsic magnetic anisotropy of a series of
82 amphiboles having a wide range of chemical compositions is characterized. The magnetic
83 anisotropy was measured in low and high magnetic fields and at different temperatures in
84 order to isolate the paramagnetic AMS. The paramagnetic AMS is then interpreted based on
85 the general crystal structure of the amphiboles and their chemical composition. A main focus
86 is put on the dependence of AMS on the Fe concentration.

87 **2. Material and methods**

88 Amphibole is an inosilicate that has the general formula $A_{0-1}B_2C_5T_8O_{22}(OH,F,Cl)_2$,
89 where *A* = Na, K; *B* = Ca, Na, Fe^{2+} , Mn, Li, Mg; *C* = Mg, Fe^{2+} , Fe^{3+} , Al, Ti, Mn, (Ni, Cr, V,
90 Li, Zn); and *T* = Si, Al. The main structural element defining amphiboles are $[(T_4O_{11})^{6-}]_n$
91 chains, i.e. double chains of tetrahedrally coordinated silica or aluminum. All tetrahedra of the
92 same double chain point in the same direction, whereas two double chains with oppositely
93 pointing tetrahedra are bonded by a band of octahedrally coordinated cations (*C*) (Figure 1).
94 These cations occupy one of three sites (labeled M1, M2 and M3), which possess variable
95 distortions of the octahedra, depending on the local environment. The M3 octahedra share 6
96 edges with adjacent octahedra, the M2 sites share 3 edges with octahedra and one with each of
97 the two M4 polyhedra. M1 shares 5 edges with octahedra and 1 with the M4 polyhedron. The
98 sizes of the M1, M2 and M3 sites depend on the radius of the cation a given site hosts.
99 Additionally, the sizes of M1 and M3 octahedra are also influenced by the amount of $(OH)^-$
100 substitution by F^- and Cl^- . The two tetrahedral double chains and the octahedral strip form so-
101 called I-beams. Neighboring I-beams are bonded by cations in M4 (*B*) and *A* sites. The

102 cations in the M4 sites have usually a higher than 6-fold coordination, and the coordination
103 number is determined by the size of the cation. The A-site is coordinated by 12 surrounding
104 oxygen atoms and can be vacant, partially occupied or filled.



105

106 *Figure 1. Crystal structure and site locations for amphiboles (figure generated using*
107 *CrystalMaker).*

108

109 Amphiboles are subdivided into 4 main groups, according to the main M4- or B-cation.
110 Amphiboles that are classified as calcic (1), calcic-sodic (2) or sodic (3) have large cations,
111 Ca and Na, in varying proportions, in the M4 sites. The M4 site in the Fe-Mg-Mn amphiboles
112 (4) is occupied by smaller cations. Depending on the size of the cations in the M4 sites, the
113 stacking sequence changes and thus amphiboles can possess a monoclinic or orthorhombic
114 unit cell. Clinoamphiboles (space group $C2/m$) are more common than orthoamphiboles

115 (*Pnma*). The symmetry elements as defined by the space groups can dictate the orientation of
116 principal susceptibility directions according to Neumann's principle (Neumann 1885), which
117 states that any physical property of a crystal has to include all symmetry elements of its space
118 group. Therefore, each principal susceptibility has to be parallel to one of the crystallographic
119 axes for the orthoamphiboles, while for clinoamphiboles one principal susceptibility has to be
120 parallel to the crystallographic *b*-axis (Nye 1957).

121 With respect to the magnetic properties, it is the location and arrangement of Fe atoms
122 that will be of greatest importance. This is due to the large magnetic moment of Fe in
123 combination with a relatively high abundance in the crystal lattice. Iron can be present as Fe²⁺
124 or Fe³⁺, whereby the Fe³⁺/Fe²⁺ ratio rarely exceeds 1/2. Exceptions to this general rule can be
125 found in Fe-rich hornblende (often referred to as oxy-hornblende) and hastingsite. In
126 actinolite, Fe²⁺ prefers M1 and M3 over M2, and some Fe²⁺ can also be located at M4 (Deer et
127 al. 1997). Hornblende generally shows a similar Mg/Fe ratio in each of the M1, M2 and M3
128 sites, and Fe²⁺ can be located in M4. Fe³⁺, like other small cations (e.g. Ti, Al), is
129 preferentially located at the M2 sites (Deer et al. 1997). Metamorphic and skarn hornblende
130 are different; in these minerals, Mg shows a preference for M2 and Fe has a tendency to be
131 located in M1 or M3. In richterite, Fe²⁺ is enriched in the M2 sites compared to the M1 or M3
132 sites, where the Fe/Mg ratios are similar. If Mn is present, it occupies the M4 or M2 sites. In
133 contrast, Fe²⁺ prefers M1 and M3 in riebeckite, where some Fe²⁺ can also enter M4. Fe³⁺ in
134 riebeckite is located in M2 sites. In the anthophyllite-gedrite series, Fe²⁺ shows a preference
135 for M4 over M1, M2 and M3, which possess similar Fe²⁺ concentrations. If there is a
136 difference between M1, M2 and M3, the Fe²⁺ concentration is lowest in M2. When OH is
137 substituted by F or Cl, this can also influence the site occupancy; Fe-F avoidance forces a
138 larger proportion of Fe²⁺ into the M2 sites, whereas Cl prefers bonds to Fe²⁺ over bonds to

139 Mg, which results in a preferential ordering of Fe²⁺ into the M1 and M3 sites (Deer et al.
140 1997).

141 **2.1 Sample description**

142 A collection of 28 natural single crystals and one aggregate was analyzed, chosen to
143 cover a broad range of chemical compositions (Table 1). These include crystals from the
144 calcic amphiboles (tremolite, actinolite and hornblende groups), sodic-calcic (richterite) and
145 sodic (riebeckite) (clino-)amphiboles and one Fe-Mn-Mn orthoamphibole (gedrite). The
146 individual crystals and the aggregate were cleaned with ethanol in an ultrasonic cleaner and
147 oriented prior to measurements. Crystals were oriented based on Laue X-ray diffraction,
148 performed at the Laboratory of Crystallography, ETH Zurich. Laue images were analyzed
149 with the OrientExpress 3.4 crystal orientation software (Laugier and Filhol 1983). The
150 oriented crystals were glued into diamagnetic plastic cylinders with no magnetic anisotropy.
151 The crystallographic a^* (or a for the orthoamphibole), b and c directions corresponded to the
152 sample x , y and z -axes, respectively for magnetic measurements. The accuracy of crystal
153 orientation is $\pm 5^\circ$. For the riebeckite aggregate, only the c -axis, which corresponds to the
154 long axis of individual fibrous crystals, was oriented.

155 **2.2 Chemical analysis**

156 Bulk chemical composition was determined using laser ablation inductively coupled
157 plasma mass spectrometry (LA-ICP-MS) at the Institute of Geological Sciences, University of
158 Bern. Because most crystals could not be modified (e.g. for producing polished sections), the
159 analyses were performed on crystal surfaces or cleavage planes, and for some crystals also on
160 polished cross-sections (cf. Table A). LA-ICP-MS was preferred over electron probe
161 microanalysis (EPMA) because LA-ICP-MS samples a bigger volume (here a cylinder of 90
162 μm diameter and about 60 μm depth). Hence minute impurities that may greatly affect the
163 magnetic properties, such as exsolutions, melt or mineral inclusions, are also comprised in the

164 mineral analysis. Notably metamorphic amphiboles often contain mineral inclusions, referred
165 to as poikilitic growth. Per sample, four to six analyses were performed to obtain information
166 on element homogeneity, expressed as one standard deviation (SD) in Table A (online
167 supplementary).

168 The LA-ICP-MS used consists of a GeoLas Pro system coupled with an Elan DRC-e
169 ICP-MS, optimized following procedures detailed in Pettke et al. (2012). SRM610 from NIST
170 was used as the external standard material, with preferred values reported by Spandler et al.
171 (2011). Data reduction employed SILLS (Guillong et al. 2008), and internal standardization
172 was done by normalizing to 98 wt% total major oxides, thus allowing for 2 wt% of OH, F or
173 Cl that cannot be measured with LA-ICP-MS. Data are considered to be accurate to better
174 than 2 % 1 SD. The analytical accuracy is thus insufficient to reliably quantify Fe³⁺ and Fe²⁺
175 by LA-ICP-MS.

176 In order to determine the relative proportions of Fe²⁺ and Fe³⁺ and help in assigning the
177 Fe to the various crystallographic sites Mössbauer spectra were measured on selected samples
178 at the Department of Chemistry, University of Copenhagen. Absorbers were prepared by
179 mixing powdered mineral samples and boron nitride into Perspex^R sample holders. Spectra
180 were obtained at room temperature using a conventional constant acceleration spectrometer
181 with the absorber perpendicular to the γ -ray direction and samples FAkt1 and FAkt4 were
182 also measured at the magic angle (tilted at 54.7° relative to the γ -rays), to remove effects of
183 mineral alignment in the powder. The spectrometer was calibrated using the spectrum of a
184 thin foil of natural Fe at room temperature, and isomer shifts are given relative to the center of
185 this absorber. All spectra exhibit three absorption lines which are interpreted as being
186 composed of three overlapping doublets: one due to Fe³⁺ and two due to Fe²⁺. The maximum
187 intensities of the absorption lines were between 3% and 7% and baseline counts in the folded
188 spectra were between 2 and 10 million counts. Lines were deconvoluted assuming Lorentzian

189 lineshape and constraining the lines of each component to be identical. This constraint could
190 not be applied to samples FAkt1 and FAkt4 due to preferred orientation of the grains in the
191 powdered sample. New absorbers were prepared and measured using the magic angle and
192 these spectra were suitable for the constraints (equal width and intensity of the two lines in
193 the doublet). Assuming identical f-factors for each of the Fe components, the relative spectral
194 areas were converted into abundances. The samples were scanned using amplitudes of 5 and
195 12 mm/s to achieve good spectral resolution of the amphibole components and to allow for
196 checking for the presence of inclusions of magnetically ordered Fe oxides.

197 Site occupancies for individual cations were then determined based on the general
198 formula $A_{0-1}B_2C_5T_8O_{22}(OH,F)_2$. Because the A site can be vacant or partially filled, the
199 recalculation is not straightforward, unless the Fe^{2+}/Fe^{3+} ratio is known. For each sample, one
200 of the following three models was used:

201 (1) When Mössbauer data were available, i.e., the Fe^{3+} and Fe^{2+} concentrations are
202 known, the site distribution was defined based on a charge balance, setting the total
203 number of cation charges to 46.

204 (2) For orthoamphiboles, it was assumed that no Na is located in M4. In this case, the
205 number of cations minus Na and K equals 15.

206 (3) For clinoamphiboles, it was assumed that no Mg, Mn or Fe^{2+} occupy the M4 site and
207 the total number of cations minus Ca, Na and K is equal to 13.

208 **2.3 Magnetic measurements**

209 **Characterization of ferromagnetic inclusions.** All magnetic measurements were made
210 at the Laboratory for Natural Magnetism, ETH Zurich. Acquisition of isothermal remanent
211 magnetization (IRM) was measured on selected samples in order to check for the presence of
212 and identify ferromagnetic inclusions within the crystals. Samples were magnetized along the

213 –z direction with an ASC Scientific IM-10-30 Pulse Magnetizer in a field of 2 T.
214 Subsequently, the sample was remagnetized along the +z direction in increasing fields
215 between 20 mT and 2 T. After each magnetization step, the IRM was measured on a 2G
216 Enterprises, three-axis cryogenic magnetometer, Model 755.

217 **Low-field AMS and mean mass susceptibility.** Magnetic susceptibility can be
218 described by a symmetric second-order tensor with eigenvalues $k_1 \geq k_2 \geq k_3$, or $|k_1| \geq$
219 $|k_2| \geq |k_3|$ in the case of diamagnetic samples, i.e. k_1 corresponds to the most and k_3 to the
220 least negative susceptibility for diamagnetic samples (Hrouda 2004). The corresponding
221 eigenvectors define the directions of the principal susceptibilities. This can be represented by
222 a magnitude ellipsoid of susceptibility, often referred to as anisotropy ellipsoid. The ellipticity
223 can be described by the AMS degree $P = k_1/k_3$, or k'
224 $= \sqrt{[(k_1 - k_{mean})^2 + (k_2 - k_{mean})^2 + (k_3 - k_{mean})^2]}/3$, where $k_{mean} = (k_1 + k_2 + k_3)/3$ and
225 AMS shape $U = (2k_2 - k_1 - k_3)/(k_1 - k_3)$ (Jelinek 1981, 1984). Low-field AMS was measured on
226 an AGICO MFK1-FA susceptibility bridge. Measurements were performed at a frequency of
227 976 Hz and in a field of 200 A/m, or 500 A/m for samples with weak susceptibility. The low-
228 field AMS was determined using a 15-position measurement scheme, in which every position
229 was measured 10 times to increase the signal quality. This allows for an estimate of data
230 quality, described by R_I , which is defined as the ratio between the deviation of the AMS
231 ellipsoid from a sphere and noise level (cf. Biedermann et al. 2013). With the low-field
232 method, the superposition of diamagnetic, paramagnetic and ferrimagnetic anisotropies are
233 determined. The mean susceptibility was determined from the mass-normalized directional
234 measurements and is referred to as mass susceptibility.

235 **High-field AMS.** High-field AMS was measured on a torque-meter (Bergmüller et al.
236 1994). Torque was measured while rotating the sample sequentially in three mutually
237 orthogonal planes at 30° increments. Measurements were conducted in six different fields

238 between 1.0 and 1.5 T and at two temperatures, room temperature (RT) and 77 K. For
239 samples having weak torque signals, e.g. tremolite, the measurements were repeated in a more
240 accurate mode and with 15° increments. The different temperature- and field-dependencies of
241 diamagnetic, paramagnetic and ferrimagnetic contributions allow separation of the individual
242 components of the high-field AMS (Martín-Hernández and Hirt 2001, 2004; Schmidt et al.
243 2007b). The method of defining the relative contributions and errors of the paramagnetic and
244 ferromagnetic components to the AMS is described in Martín-Hernández and Hirt (2001). The
245 paramagnetic susceptibility and its anisotropy increase with decreasing temperature. This
246 increase can be quantified by the p_{77} -factor: $p'_{77} = k'(77\text{K})/k'(\text{RT})$.

247 **Low-temperature magnetization curves.** Susceptibility was measured as a function of
248 temperature and crystallographic direction in three crystals. In addition, hysteresis loops were
249 measured at several temperatures to check for the field-dependence of the susceptibility.
250 These measurements were made on a Quantum Design Magnetic Property Measurement
251 System (MPMS) at the Laboratory for Solid State Physics, ETH Zurich. The crystals were
252 cooled from room temperature to 2 K, during which the magnetization was measured every 10
253 K initially and in 1 K steps at low temperatures; temperature was stabilized before each
254 measurement point. Measurements were made in a weak field of 10 mT to investigate if the
255 crystals undergo magnetic ordering at low temperature. The same magnetization vs.
256 temperature measurements were then repeated in a strong field of 1 T, to understand in detail
257 the increase in the degree of anisotropy that is observed in the high-field AMS measurements
258 at 77 K. At sufficiently high temperature, the susceptibility vs. temperature data could be
259 fitted with a Curie-Weiss model for paramagnetic materials $\chi_{obs} = \mu_0 C/(T-\theta) =$
260 $\mu_0 \mu_B^2 g^2 S(S+1)N/(3k_b(T-\theta))$, where χ_{obs} is the molar susceptibility, $\mu_0 = 4\pi \times 10^{-7}$ Vs/(Am) the
261 permeability of free space, C the Curie constant, T the measurement temperature, θ the
262 ordering temperature, μ_B is the Bohr magneton, g is Landé's g -factor, S is the spin number, N

263 is the number of magnetic ions, and k_b is Boltzmann's constant. Ferrous Fe possesses a spin S
264 = 2 and ferric Fe possesses a spin S of 5/2. Landé's g-factor and the ordering temperature θ
265 depend on crystallographic direction and were determined based on the Curie-Weiss fits.

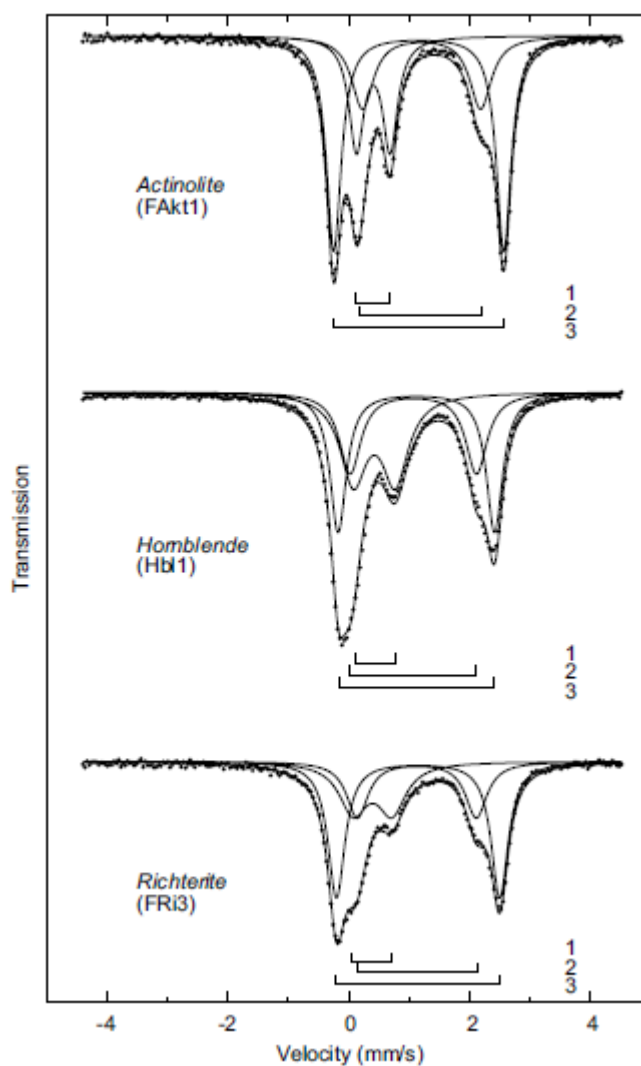
266 3. Results

267 3.1 Chemical composition

268 **Bulk composition.** Average chemical compositions of the samples and site occupancies
269 are given in Tables A and B (online supplementary). For most crystals, the spot-to-spot
270 variability is small, thus indicating homogeneous element distribution throughout the crystal
271 and thus little growth zonation. Some crystals, however, show zonations of e.g. Al, K, Na or
272 Fe. One sample, NMB535, was too big to fit the ablation chamber and could thus not be
273 analyzed by LA-ICP-MS. A few samples, e.g. Amph1 or NMB44662, show too high T-site
274 SiO₂ occupancies. For Amph1, where only EPMA data are available, we lack an explanation
275 for the apparent high SiO₂ concentration. The riebeckite sample, NMB44662, represents an
276 aggregate of crystals that may contain melt or mineral inclusions or intercrystal minerals. The
277 presence of such impurities is indicated by the considerably higher variability in major
278 element concentrations when compared with the other amphibole analyses. The samples cover
279 a range of chemical compositions, and the Fe concentrations vary between 0.03 and 25.5 wt%
280 FeO. Other magnetic cations are present only in small amounts (0.01 – 1.1 wt% MnO, 5 –
281 1400 µg/g Cr, 0.8 – 920 µg/g Ni, and 0.01 – 65 µg/g Co) and thus have negligible
282 contributions to the overall magnetic properties.

283 **Mössbauer spectroscopy.** Mössbauer analysis shows that all analyzed samples contain
284 three doublets, one of which can be assigned to Fe³⁺, which we refer to as Component 1, and
285 two to high-spin Fe²⁺, which are referred to as Component 2 and 3 (Figure 2, Table 2). Peak
286 assignment is not straightforward due to the chemical variation in amphiboles, which causes

287 the Mössbauer spectra to vary considerably between mineral types (e.g. Hawthorne 1983).
 288 Component 1 has an isomer shift between 0.36 mm/s and 0.45 mm/s, a quadrupole splitting
 289 between 0.26 mm/s and 0.78 mm/s, and a line width between 0.22 mm/s and 0.60 mm/s. The
 290 line widths are much smaller for tremolite and actinolite, indicating one unique site M2 for
 291 Fe^{3+} , but larger for hornblende and richterite, which may arise if Fe^{3+} is distributed over M1,
 292 M2 and M3 sites or if there is substitution of OH^- by O^{2-} , causing changes in the local
 293 environment at the M2 site.



294

295 *Figure 2. Characteristic Mössbauer spectra and fits for selected amphibole crystals. Numbers*
 296 *refer to Components 1, 2 and 3 discussed in the text and shown in Table 2.*

297

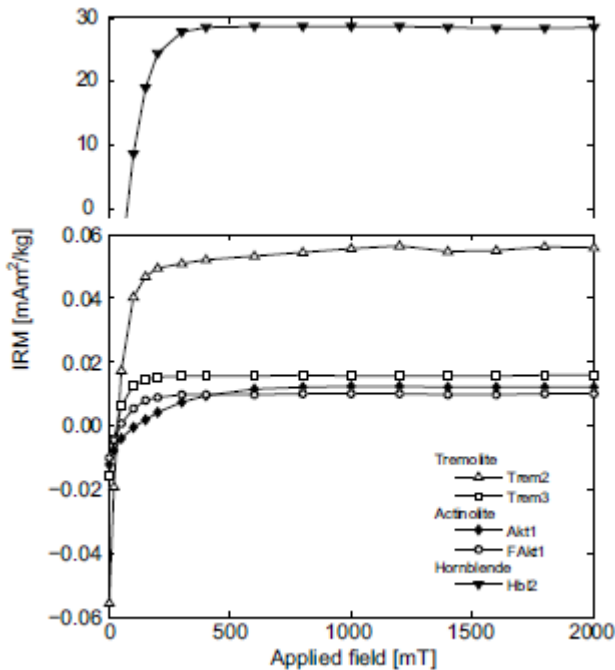
298 Component 2 has an isomer shift between 1.06 mm/s and 1.15 mm/s, a quadrupole
299 splitting between 1.92 mm/s and 2.18 mm/s, and a line width between 0.41 mm/s and 0.47
300 mm/s. Component 3 has an isomer shift between 1.11 mm/s and 1.16 mm/s, a quadrupole
301 splitting between 2.58 mm/s and 2.82 mm/s, and a line width between 0.29 mm/s and 0.34
302 mm/s. The large line widths of Component 2 could indicate that there are unresolved doublets
303 from more than one site; alternatively, they may result from variations in the local
304 environment of a single site. Several studies have proposed different peak assignments, based
305 on the observed variation in isomer shift and quadrupole splitting (Abdu and Hawthorne
306 2009; Hawthorne 1983; Oberti et al. 2007). In the present study, Component 2 is assigned to
307 Fe²⁺ that occupies the M2 site, in accordance with Reusser (1987) who shows that the
308 quadrupole splitting in M2 lies in-between that of M1/M3 and M4.

309 The Fe²⁺/Fe³⁺ ratio is lowest in the hornblende samples, ranging from 1.0 to 1.8, and
310 highest in the tremolite with a ratio of 6.5 (Table 2). The actinolites possess Fe²⁺/Fe³⁺-ratios
311 of 2.8 and 3.3, and the three richterites have Fe²⁺/Fe³⁺-ratios between 2.1 and 2.7. It should be
312 noted that no magnetically ordered components could be detected in the wide amplitude scans
313 in any crystal, except for Amph3. The Mössbauer spectrum of Amph3 shows two sextets
314 indicating a ferrimagnetic contribution from non-stoichiometric magnetite.

315 **3.2 IRM acquisition**

316 Acquisition of IRM shows that magnetization increases rapidly in low fields, which
317 indicates that these crystals contain a low coercivity mineral, such as magnetite or its
318 weathering product maghemite (Figure 3). The IRM of some crystals, e.g. Trem3, Hbl2 and
319 FAkt1 is saturated by 200 mT, indicating that only a low coercivity phase is present. In other
320 crystals, e.g. Trem2 and Akt1, saturation IRM is approached more slowly, which suggests that
321 a high coercivity mineral such as hematite may also be present. The coercivity of remanence,
322 which is affected by the type of ferromagnetic inclusions within the crystals, varies between

323 40 and 120 mT, whereby it is highest in Akt1 for which the IRM is not completely saturated.
 324 The amount of the high coercivity component is relatively small and should not influence the
 325 torque signal. The low coercivity component, however, is significant in some crystals and
 326 thus needs to be separated in order to obtain the paramagnetic anisotropy.



327

328 *Figure 3. Acquisition of IRM for representative samples. Note the different scale for*
 329 *hornblende compared to the other amphibole minerals.*

330

331 3.3 Mass susceptibility

332 Mass susceptibility, χ_m , was determined from the low-field anisotropy measurements,
 333 and ranges from $-3.5 \times 10^{-8} \text{ m}^3/\text{kg}$ to $2.6 \times 10^{-6} \text{ m}^3/\text{kg}$. All tremolite and two of the richterite
 334 crystals (FRi4, FRi5) are diamagnetic. In order to assess if ferromagnetic inclusions are
 335 affecting the susceptibility of the remaining crystals, the measured values are compared with
 336 the theoretical paramagnetic susceptibility that can be derived from the chemical composition.

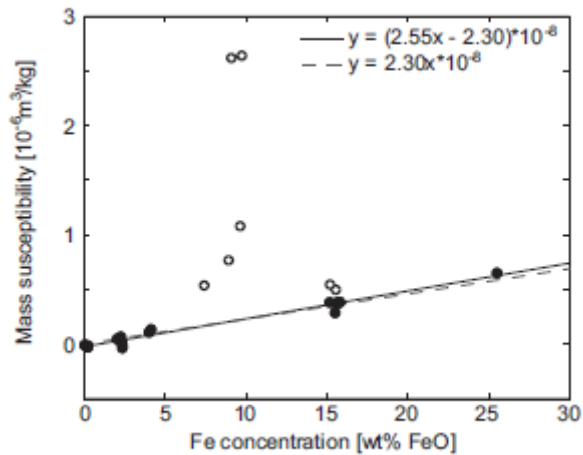
337 According to Langevin theory, mass susceptibility can be given by $\chi_m = \mu_0 \frac{(L\mu_B)^2}{3RT} (\alpha n_\alpha^2 +$
 338 $\beta n_\beta^2 + \dots)$, where L is Avogadro's number, R is the gas constant, $\alpha, \beta \dots$ are the molar

339 amounts of the paramagnetic ions, and n_α , n_β ... are the magnetic moments of the respective
340 ions given in terms of μ_B (Bleil and Petersen 1982). Manganese, Cr, Ni, and Co
341 concentrations are low in all samples, and only Fe is present in large enough quantities to
342 make a significant contribution to the mass susceptibility. Therefore, only Fe is used in the
343 theoretical calculation, which assumes the cations are in the divalent form, and that there is no
344 interaction between the magnetic moments of the cations.

345 Fifteen crystals show a good agreement between the measured and theoretical
346 paramagnetic susceptibility (Table 3). Crystals FAKt4, FAKt7, Amph, Amph3, Amph5, Hbl1
347 and Hbl2, however, show a significant difference that can be attributed to ferromagnetic
348 inclusions. Figure 4 shows the relationship between Fe concentration and mass susceptibility.
349 There is a good linear relationship for the group of crystals that do not contain a significant
350 amount of ferromagnetic inclusions, demonstrating that the mass susceptibility can be
351 quantitatively related to paramagnetic cations. The data can be fit by the relationship

$$352 \quad \chi_m = (2.55 \times Fe - 2.30) \times 10^{-8} \text{ m}^3/\text{kg} \quad (\text{Eq. 1})$$

353 where Fe is the Fe concentration in wt%, assuming for simplicity that all Fe is Fe^{2+} . The
354 offset is close to the value of diamagnetic susceptibility of the tremolite crystals, and the fit is
355 in agreement with the theoretical increase of $2.30 \times 10^{-8} \text{ m}^3/\text{kg}$ per wt% FeO.



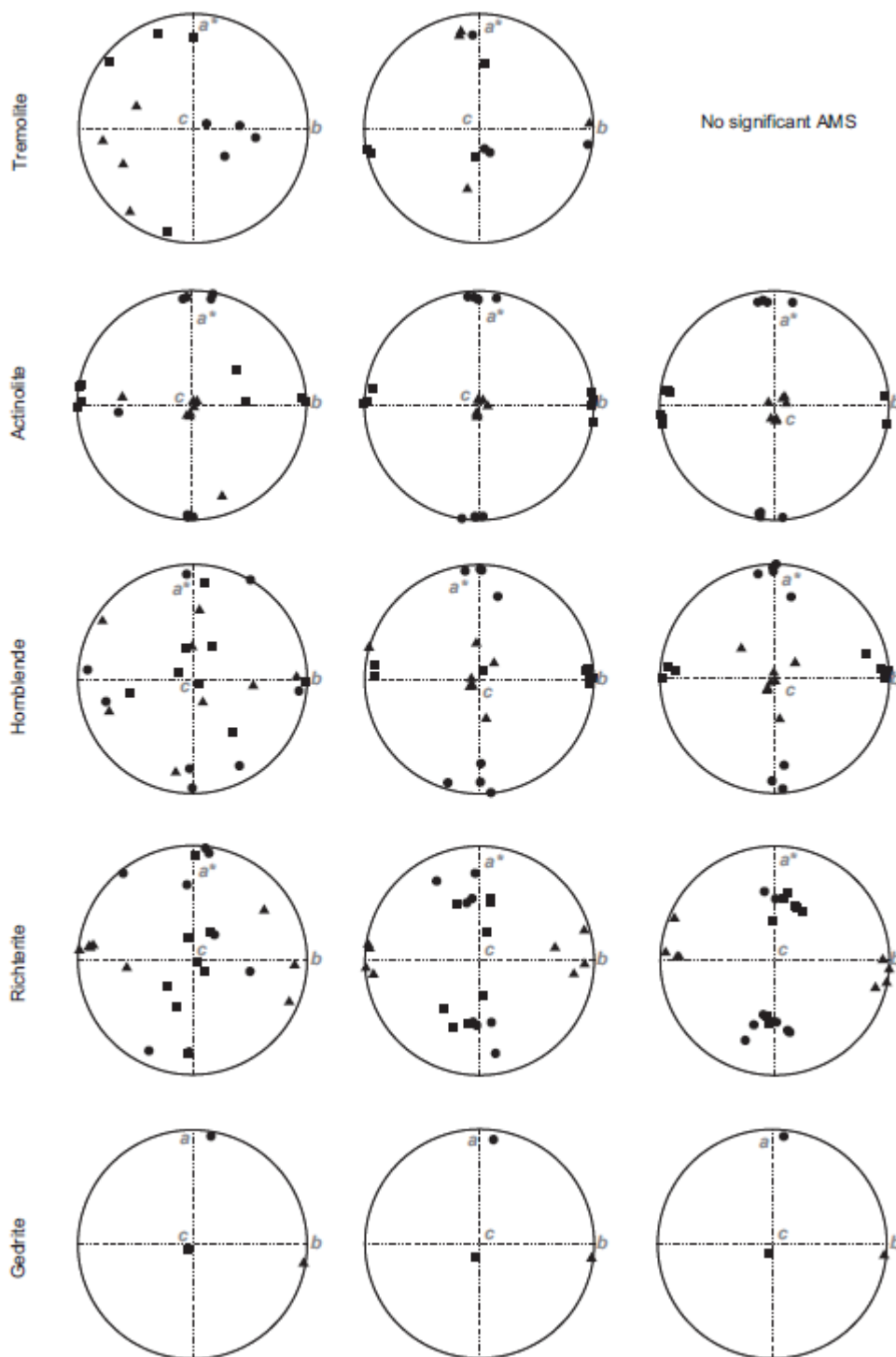
356

357 *Figure 4. Mass susceptibility as a function of Fe concentration. Open circles represent*
 358 *samples with significant ferromagnetic contributions from mineral or melt inclusions.*
 359 *Samples represented by filled circles are considered purely paramagnetic or diamagnetic.*
 360 *Solid and dashed lines represent the susceptibility increase as defined by Eq. 1, and the*
 361 *theoretical increase, respectively.*

362

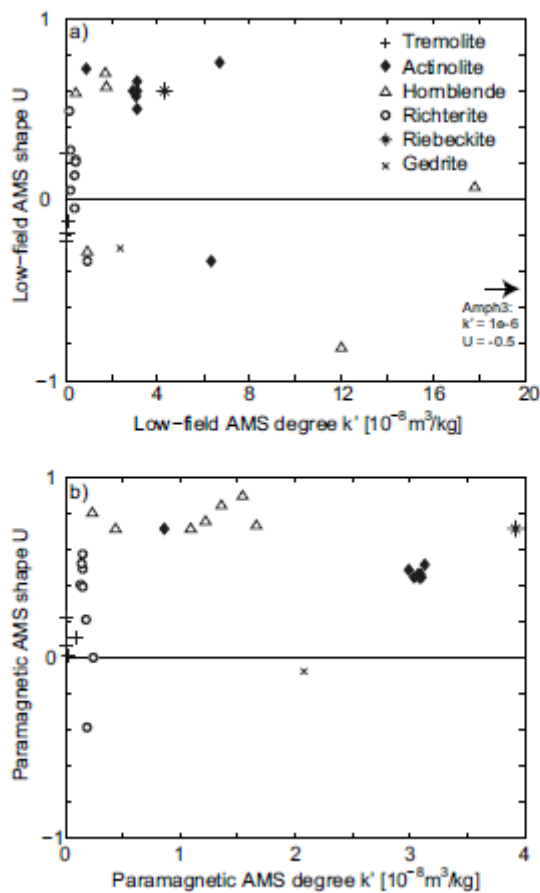
363 **3.4 Low- and high-field magnetic anisotropy**

364 The low- and high-field AMS are given in Tables 3 and 4. The diamagnetic and
 365 paramagnetic components extracted from high-field measurements can be attributed to the
 366 arrangement of cations in the silicate lattice, whereas the ferromagnetic component is related
 367 to Fe oxide inclusions or exsolutions. Figure 5 shows the directions of the principal
 368 susceptibilities of each mineral group for the low-field AMS and the dia-/paramagnetic part of
 369 the high-field AMS. The torque signal of most samples is dominated by the dia-/paramagnetic
 370 component. There is no systematic preference in the orientation of the ferromagnetic
 371 anisotropy for those samples with significant ferromagnetic content, indicating the presence
 372 of randomly oriented inclusions rather than exsolution features. The shape-factor (U) of the
 373 AMS ellipsoid is shown in Figure 6 as a function of degree of anisotropy, k' .



374

375 *Figure 5. Lower hemisphere equal-area stereoplots showing the directions of principal*
 376 *susceptibilities for minerals in the amphibole group. Left column shows principal directions of*
 377 *the low-field AMS, middle and right column are paramagnetic principal directions isolated*
 378 *from high-field data at room temperature (RT) and 77 K, respectively. Susceptibility directions*
 379 *are given in a crystallographic reference frame.*



380

381 *Figure 6. Modified Jelinek plot showing AMS shape U as a function of k' for (a) low-field AMS,*
 382 *and (b) dia-/paramagnetic AMS extracted from high-field AMS.*

383

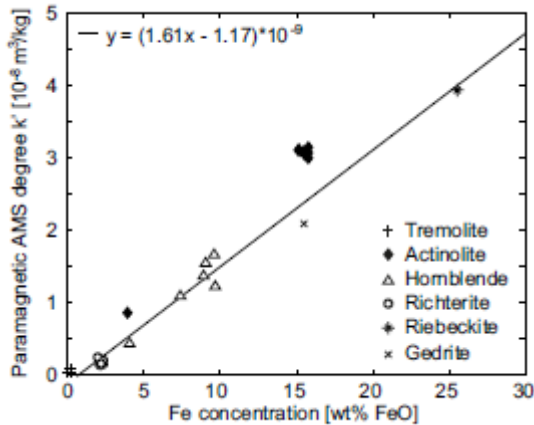
384 **Tremolite group.** The low-field AMS of tremolite is marginally significant, with R_1
 385 between 0.4 and 2.2, and it cannot be excluded that the measured AMS directions are
 386 influenced by the holder signal (cf. Biedermann et al. 2013). The high-field AMS, despite the
 387 weak torque signal, shows some relationship to the crystallographic axes (Figure 5). Trem3
 388 and Trem4 show similar directions with k_1 aligned along the crystallographic b -axis, but
 389 Trem1 has the k_2 axis and Trem2 k_3 along the b -axis. The degree of anisotropy (k') of the dia-
 390 /paramagnetic AMS is very small, ranging from $1.53 \times 10^{-10} \text{ m}^3/\text{kg}$ to $8.92 \times 10^{-10} \text{ m}^3/\text{kg}$. The
 391 shape of the AMS ellipsoid is neutral, but oblate (Figure 6). The high-field torque signal is
 392 dominated by noise at 77 K. This deterioration in the torque response suggests that the

393 diamagnetic susceptibility may be responsible for the observed AMS at room temperature,
394 because the susceptibility becomes more isotropic with the enhancement of the paramagnetic
395 susceptibility at 77 K.

396 **Actinolite group.** The Fe-concentration controls the susceptibility in the actinolite and
397 ferroactinolite crystals. The principal directions of the low-field AMS have k_1 along the
398 crystallographic b -axis, k_2 along the crystallographic c -axis, and k_3 along the crystallographic
399 a^* -axis, in all crystals except FAkt4 and FAkt7, which contain ferromagnetic inclusions
400 (Figure 5). The principal axes become even better grouped for all crystals, when the
401 paramagnetic AMS is isolated in high fields either at room temperature or at 77 K. Due to the
402 lower Fe-concentration, k' is significantly lower in Akt1 compared to the ferroactinolites,
403 which have k' around $3 \times 10^{-8} \text{ m}^3/\text{kg}$ (Figure 6). The shape of the AMS is oblate in all crystals,
404 but slightly more oblate in Akt1, compared to the ferroactinolite, in which U is around 0.46.
405 The factor p'_{77} is lowest in Akt1 with $p'_{77} = 7.75$, and between 9.47 and 11.15 for the
406 ferroactinolite crystals.

407 **Hornblende group.** The orientation of the principal axes for the low-field AMS is
408 scattered in relation to crystallographic axes in the crystals from the hornblende group, due to
409 the significant ferromagnetic contribution to the susceptibility. The paramagnetic AMS,
410 however, shows a similar orientation of its principal axes as found for actinolite, with k_1
411 parallel to the crystallographic b -axis, k_2 to the c -axis and k_3 to the a^* -axis in most samples
412 (Figure 5). The same general relationship between eigenvectors and crystallographic axes is
413 evident at 77K. For Amph3, the k_1 and k_2 axes are inverted at room temperature, but not at 77
414 K. It is interesting to note that the crystal with the lowest Fe-concentration, Amph1, shows the
415 largest deviation of the k_2 and k_3 axes in the plane of the crystallographic a - and c -axes. The
416 crystals in the hornblende group show the largest spread in k' , ranging from $2.39 \times 10^{-9} \text{ m}^3/\text{kg}$
417 to $1.66 \times 10^{-8} \text{ m}^3/\text{kg}$, and k' generally increases with increasing Fe-concentration (Figure 7).

418 The AMS ellipsoid is more oblate, compared to the ferroactinolite crystals, with U between
 419 0.71 and 0.89. p'_{77} is between 7.29 and 8.97.



420

421 *Figure 7. Paramagnetic anisotropy degree k' as a function of Fe concentration.*

422

423 **Richterite group.** Although the richterite crystals all have a similar Fe concentration,
 424 their mass susceptibility is highly variable, and FRi4 and FRi5 are diamagnetic. The principal
 425 axes of the low-field AMS ellipsoid show almost no relationship to the crystallographic axes.
 426 The dia-/paramagnetic component of the high-field AMS shows that the k_2 axes are generally
 427 along the crystallographic b -axis, and the k_1 and k_3 in the plane of the a - and c -axes. At 77 K,
 428 there is a better grouping of all three axes with k_1 and k_3 approximately 45° from the c -axis.
 429 The degree of anisotropy is very similar in all crystals, and is between $1.35 \times 10^{-9} \text{ m}^3/\text{kg}$ and
 430 $2.40 \times 10^{-9} \text{ m}^3/\text{kg}$. The shape, however, is highly variable ranging from prolate to oblate. p'_{77} is
 431 between 5.25 and 9.86.

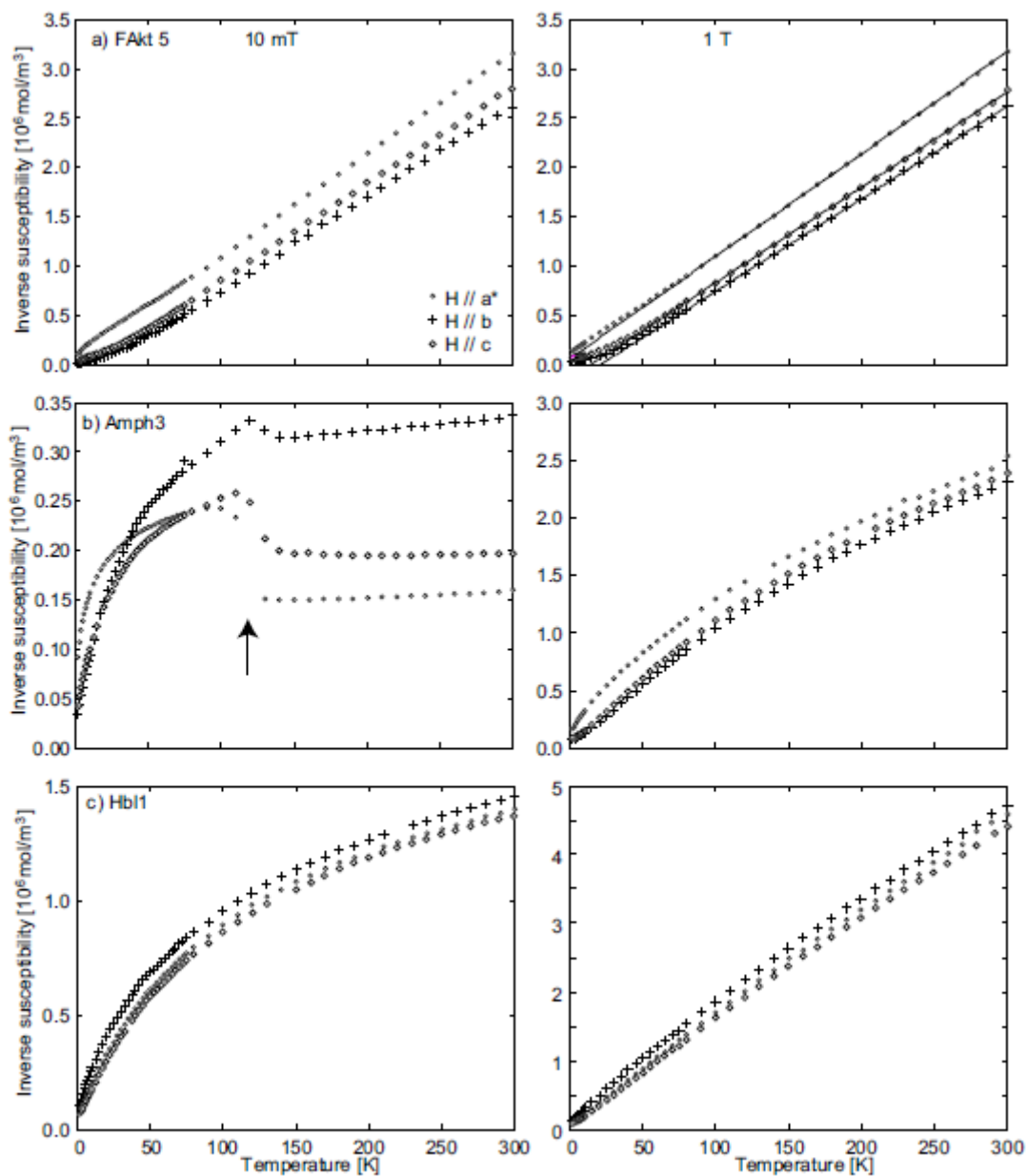
432 **Riebeckite.** The riebeckite sample is not a single crystal, but consists of an aggregate of
 433 fibrous grains, in which the fibers were all oriented along one direction. The maximum
 434 susceptibility is parallel to the long direction of the fibers. Because the magnetic anisotropy
 435 cannot be related to a single crystal, the orientations of the principal axes are not given. The

436 principal susceptibilities provide a minimum estimate for the anisotropy, as the individual
437 fibers may not be perfectly aligned within the aggregate. The sample shows the highest degree
438 of anisotropy with $k' = 3.92 \times 10^{-8} \text{ m}^3/\text{kg}$, and a U of 0.71, which is comparable to the crystals
439 from the actinolite and hornblende groups. The p'_{77} -factor is high with a value of 13.4.

440 **Gedrite.** The gedrite crystal has k_1 parallel to the crystallographic c -axis, k_2 parallel to
441 the b -axis, and k_3 parallel to the a -axis both in low-field and high-field (Figure 5). The degree
442 of anisotropy equals $k' = 2.08 \times 10^{-8} \text{ m}^3/\text{kg}$, the shape is weakly prolate with $U = -0.08$, and
443 $p'_{77} = 8.12$.

444 **3.5 Low-temperature magnetic properties**

445 The inverse of the susceptibility is shown in as a function of temperature, crystal
446 orientation and applied field in Figure 8. The paramagnetic susceptibility dominated the
447 induced magnetization in the 1 T field, in which the ferromagnetic component is saturated.
448 The susceptibility in actinolite FAkt5 follows an inverse linear relationship with temperature
449 for $T > \sim 100 \text{ K}$ (Figure 8a). Below this temperature, local ferromagnetic ordering sets in when
450 the applied field is along b or c , and local antiferromagnetic interactions occur when the
451 applied field is parallel to a^* . A Curie-Weiss fit to the paramagnetic range indicates
452 paramagnetic Curie temperatures of -6 K, 21 K and 14 K in the a^* , b , and c directions,
453 respectively. Landé's g -factor is between 2.4 and 2.5, indicating an orbital contribution to the
454 magnetic moment. Both hornblende samples are strongly affected by ferromagnetic inclusions
455 in the crystals, as seen from the non-linearity of the inverse susceptibility as a function of
456 temperature (Figure 8b, c). A Verwey transition is observed in Amph3 (Verwey 1939; Walz
457 2002).



458

459 *Figure 8. Low-temperature magnetization curves for selected samples. Symbols correspond*
 460 *to measured susceptibility along the a*, b and c crystallographic axes. Solid lines are the*
 461 *corresponding Curie-Weiss fits. The black arrow indicates a magnetic transition in Amph3.*

462

463 **4. Discussion**

464 **4.1 Mass susceptibility and composition**

465 Vernon (1961) demonstrated that the mass susceptibility of paramagnetic minerals
466 correlates with the concentrations of Fe^{2+} and Mn, which agrees with our dataset when
467 ferromagnetic inclusions in the crystals are negligible. Parks and Akhtar (1968) reported that
468 the effective magnetic moment of Fe is strongly influenced by the crystal field, i.e. site
469 symmetry, dimension or interatomic distance, and the type of bonding. They calculated an
470 effective magnetic moment $n_{\text{Fe}^{2+}} = 6.42$. The data presented here suggest a lower value of 5.5
471 to 5.6, a value that is in accordance with theoretical and experimental limits on the magnetic
472 moment of Fe^{2+} (Parks and Akhtar 1968; Vernon 1961).

473 A linear relationship is observed between Fe concentration in the crystals and measured
474 susceptibilities in the absence of ferromagnetic inclusions. Therefore, mass susceptibility can
475 be used to deduce Fe-concentration, using the formula in Equation 1.

476 **4.2 Low-field AMS and ferromagnetic inclusions**

477 The principal directions of the AMS ellipsoid are more scattered for the low-field than
478 for the high-field data. In samples whose low-field directions deviate from the paramagnetic
479 high-field directions, the low-field directions plot close to those of the ferromagnetic
480 component. Even though present in minute concentrations, the ferromagnetic inclusions
481 dominate both the mass susceptibility and its anisotropy. Since the ferromagnetic AMS does
482 not show any systematic orientation of principal susceptibilities with respect to the amphibole
483 crystal lattice, care has to be taken when interpreting low-field AMS, in particular in minerals
484 in which magnetite inclusions are expected. Whether such inclusions occur in hornblende
485 depends on the oxygen fugacity and on pressure. Magnetite is commonly found in shallow
486 calcalkaline magmatic rocks. Therefore, care has to be taken to remove the magnetic signal
487 due to these inclusions when interpreting magnetic fabrics in such rocks.

488 **4.3 Relation between AMS, crystal structure and composition**

489 Iron is not only expected to have a large influence on mass susceptibility, but also on
490 the anisotropy of the susceptibility. In addition to concentration, the oxidation state and site
491 distribution of Fe are important determining factors for the susceptibility anisotropy. Site
492 distribution could have an effect in either of two ways: (1) different crystallographic sites
493 have different distortions and local environments and therefore varying crystal fields, which
494 may influence the ionic anisotropy of Fe, and (2) crystallographic sites are arranged along
495 preferred axes or in planes, which defines the distances between nearest-neighbor Fe atoms in
496 different directions and this affects interactions between individual magnetic moments.

497 **Principal susceptibility directions.** The principal axes of the AMS ellipsoids have
498 similar orientations in actinolite and hornblende crystals (Figure 5). The only exception is
499 Amph3, in which the k_1 and k_2 axes are interchanged at room temperature. The k_3 axis is
500 parallel to a^* in all crystals, and this preference may result because a^* is normal to the plane
501 of the octahedral bands. Iron is located in these bands; therefore, dipolar interactions will be
502 smallest in the a^* direction. Another explanation can be found in crystal field theory. The
503 amphibole M1 and M3 sites have similar crystal fields to the biotite M2 and M1 sites,
504 respectively (Burns 1993). In biotite, this crystal field causes an easy-plane anisotropy with
505 the minimum susceptibility normal to the octahedral planes (Ballet and Coey 1982; Beausoleil
506 et al. 1983). A similar effect could occur in amphiboles. The k_1 axes are aligned along the
507 crystallographic b -axes, which can be explained by the fact that, within each octahedral band,
508 the distances between adjacent sites occupied by Fe is smallest in this direction. This effect
509 appears to outweigh effects caused by the orientation of the bands parallel to the c -axis.
510 Gedrite also has k_3 oriented along a , but in this case k_1 lies along the crystallographic c -axis,
511 and k_2 along the b -axis. This may be related to the different site preference of Fe^{2+} , which is
512 preferentially located in M1 - M3 in actinolite and hornblende vs. M4 in gedrite.

513 Richterite shows a grouping of k_2 about the crystallographic b -axis, and k_1 and k_3 are
514 distributed in the a - c -plane. At 77 K, the grouping of the k_2 axes along the b -axis becomes
515 stronger, and the k_1 and k_3 axes also show a grouping at an angle of approximately 45° from
516 the c -axis. At present it is not possible to explain why the principal axes show this preference.

517 The AMS of tremolite is very weak and does not show a consistent relationship with the
518 crystallographic axes when all samples are considered. Because the torque signal decreases
519 upon cooling, we surmise that paramagnetic and diamagnetic fabrics compete against one
520 another. For this reason, the magnetic anisotropy of this group will not be interpreted further.

521 **Anisotropy degree.** The paramagnetic anisotropy degree k' shows a linear increase
522 with Fe concentration (Figure 7). The actinolite crystals, however, display a slightly larger
523 degree of anisotropy than what would be expected from the trend defined by the other
524 samples. Actinolite has larger $\text{Fe}^{2+}/\text{Fe}^{3+}$ ratios than hornblende or richterite. The fact that Fe^{3+}
525 behaves isotropically while Fe^{2+} possesses an easy-plane anisotropy in a distorted octahedral
526 crystal field (Beausoleil et al. 1983), could explain the relatively stronger anisotropy in the
527 Fe^{2+} -richer actinolite. However, there is no clear correlation between the $\text{Fe}^{2+}/\text{Fe}^{3+}$ ratio and
528 the deviation of the anisotropy degree from the general trend. Furthermore, there is no
529 correlation between the ratio of the two Fe^{2+} components and deviation from the general
530 trend.

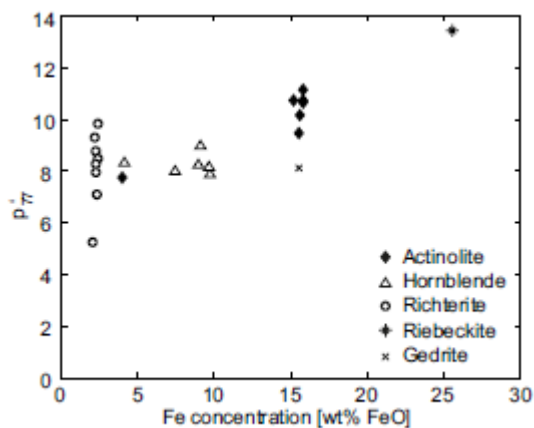
531 The tremolite, hornblende, and richterite data follow a linear trend, where

$$532 \quad k' = 1.61 \times 10^{-9} \times Fe - 1.17 \times 10^{-9} \text{ m}^3/\text{kg} \quad (\text{Eq. 2})$$

533 The fact that riebeckite exhibits the anisotropy degree predicted by this trend and its iron
534 content, suggests that all fibers have similar orientations. Gedrite, on the other hand, has a
535 lower anisotropy than expected. Possible explanations to this include differences in structure
536 and symmetry (orthorhombic as compared to monoclinic in the other amphiboles), or the fact

537 that Fe can be located in M4 sites in orthoamphiboles, whereas this site is occupied by larger
538 cations in clinoamphiboles.

539 **Temperature-dependence of the anisotropy degree.** The degree of anisotropy
540 increases by varying amounts with decreasing temperature. The factor p'_{77} is 7.8 for actinolite
541 Akt1, between 7.3 and 8.3 for hornblende, between 7 and 9 for most richterite crystals and
542 $p'_{77} = 8.1$ for gedrite (Figure 9). This is similar to p'_{77} in most minerals of the phyllosilicate
543 group (Biedermann et al. 2014a), olivine (Biedermann et al. 2014b) as well as siderite
544 (Schmidt et al. 2007a).



545

546 *Figure 9. The ratio of the anisotropy degree at 77 K to that at room temperature (p'_{77}) as a*
547 *function of Fe concentration.*

548

549 While no clear correlation appears between p'_{77} and Fe-concentration, those crystals
550 with very low or high Fe concentration tend to have larger values of p'_{77} (Figure 9). This may
551 be due to two effects. Firstly, when the diamagnetic contribution to the anisotropy is high due
552 to very low Fe concentration, an increase in the paramagnetic susceptibility appears larger.
553 Schmidt et al. (2007a) observed this effect in calcite. Secondly, the onset of local
554 ferromagnetic coupling within the octahedral bands and local antiferromagnetic coupling
555 normal to these bands at temperatures below about 100 K may also lead to a higher ratio, as

556 found in biotite (Biedermann et al. 2014a). We may expect that these interactions can only
557 occur when Fe^{2+} cations are located sufficiently close to each other; hence, this effect is seen
558 mainly in ferroactinolite with a high concentration of Fe^{2+} on the M1, M2 and M3 sites and in
559 riebeckite, with the overall largest Fe concentration.

560 **5. Implications**

561 This new comprehensive data set on single crystals of amphibole minerals with variable
562 composition and structure demonstrates that the intrinsic magnetic anisotropy is a function of
563 both chemical composition and crystal lattice. The results presented here serve as an
564 important basis for AMS studies in rocks whose AMS is dominated by amphiboles. The
565 orientation of the principal AMS axes can be used as a proxy for rock texture. The degree of
566 anisotropy in such rocks increases with (1) the strength of crystallographic preferred
567 orientation of the amphiboles, and (2) the Fe concentration within the individual crystals.
568 Thus, the AMS degree does not necessarily reflect the degree of deformation, but is related to
569 Fe concentration. The AMS appears to be independent of site occupancy in clinoamphiboles,
570 but the AMS degree increases with increasing percentage of M1, M2 and M3 sites that are
571 occupied by Fe^{2+} , which might be used for a first-order estimate of $\text{Fe}^{2+}/\text{Fe}^{3+}$ ratios.

572 The data presented in this study also highlight the influence of ferromagnetic inclusions,
573 such as individual magnetite crystals. Their presence may dominate low-field AMS and
574 override the anisotropy originating from the paramagnetic amphiboles. Consequently, a
575 separation of paramagnetic and ferromagnetic contributions to the magnetic anisotropy is
576 essential prior to determining amphibole CPO or interpreting rock texture based on magnetic
577 fabric.

578

579

580 **Acknowledgments:** A. Puschig, Natural History Museum Basel, A. Stucki,
581 Siber+SiberAathal and P. Brack and S. Bosshard, ETH Zurich are thanked for providing
582 samples for this study. D. Logvinovich helped with the Laue method for crystal orientation.
583 We are grateful to E. Reusser for assistance with recalculation of the mineral formulae.
584 W.E.A. Lorenz kindly provided support with low-temperature measurements and data
585 analysis. We thank W. Lowrie for his constructive comments. Mike Jackson and Jeff Gee are
586 thanked for their thorough reviews. This study was funded by the Swiss National Science
587 Foundation, projects200021_129806 and 200020_143438.

588

589 **References**

- 590 Abdu, Y.A., and Hawthorne, F.C. (2009) Crystal structure and Mössbauer spectroscopy of
591 tschermakite from the ruby locality at Fiskenaesset, Greenland. *The Canadian*
592 *Mineralogist* 47, 917-926.
- 593 Archanjo, C.J., Bouchez, J.-L., Corsini, M., and Vauchez, A. (1994) The Pombal granite
594 pluton: magnetic fabric, emplacement and relationships with the Brasiliano strike-slip
595 setting of NE Brazil (Paraíba State). *Journal of Structural Geology* 16, 323-335.
- 596 Ballet, O., and Coey, J.M.D. (1982) Magnetic properties of sheet silicates; 2:1 layer minerals.
597 *Physics and Chemistry of Minerals* 8, 218-229.
- 598 Beausoleil, N., Lavalley, P., Yelon, A., Ballet, O., and Coey, J.M.D. (1983) Magnetic
599 properties of biotite micas. *Journal of Applied Physics* 54, 906-915.
- 600 Bergmüller, F., Bärlocher, C., Geyer, B., Grieder, M., Heller, F., and Zweifel, P. (1994). A
601 torque magnetometer for measurements of the high-field anisotropy of rocks and
602 crystals. *Measurement Science and Technology* 5, 1466-1470.
- 603 Biedermann, A.R., Bender Koch, C., Lorenz, W.E.A., and Hirt, A.M. (2014a) Low-
604 temperature magnetic anisotropy in micas and chlorite. *Tectonophysics*, doi:
605 10.1016/j.tecto.2014.01.015
- 606 Biedermann, A.R., Pettke, T., Reusser E., and Hirt, A.M. (2014b) Anisotropy of magnetic
607 susceptibility in natural olivine single crystals. *Geochemistry Geophysics Geosystems*
608 15, 3051-3065 , doi: 10.1002/2014GC005386
- 609 Biedermann, A.R., Lowrie, W., and Hirt, A.M. (2013) A method for improving the
610 measurement of low-field magnetic susceptibility anisotropy in weak samples. *Journal*
611 *of Applied Geophysics* 88, 122-130.
- 612 Bleil, U., and Petersen, N. (1982) Magnetische Eigenschaften der Minerale, in: G.
613 Angenheister (Ed.), *Landolt-Börnstein - Numerical Data and Functional Relationships*
614 *in Science and Technology - Group V: Geophysics and Space Research*. Springer,
615 Berlin.
- 616 Borradaile, G., Keeler, W., Alford, C., and Sarvas, P. (1987) Anisotropy of magnetic
617 susceptibility of some metamorphic minerals. *Physics of the Earth and Planetary*
618 *Interiors* 48, 161-166.
- 619 Borradaile, G.J., Stewart, R.A., and Werner, T. (1993). Archean uplift of a subprovince
620 boundary in the Canadian Shield, revealed by magnetic fabrics. *Tectonophysics* 227,
621 1-15.
- 622 Burns, R.G. (1993) *Mineralogical applications of crystal field theory*, 2nd ed. 576p.
623 Cambridge University Press, UK.
- 624 Deer, W.A., Howie, R.A., and Zussman, J. (1997) *Double-chain silicates*, 2nd ed. 784p. The
625 Geological Society, London, UK.

- 626 Finke, W. (1909) Magnetische Messungen an Platinmetallen und monoklinen Kristallen,
627 insbesondere der Eisen-, Kobalt- und Nickelsalze. *Annalen der Physik* 336, 149-168.
- 628 Guillong, M., Meier, D.L., Allan, M.M., Heinrich, C.A., and Yardley, B.W.D. (2008) SILLS:
629 A MATLAB-based program for the reduction of laser ablation ICP-MS data of
630 homogeneous materials and inclusions. *Mineralogical Association of Canada Short*
631 *Course* 40, 328-333.
- 632 Hawthorne, F.C. (1983) The crystal chemistry of the amphiboles. *The Canadian Mineralogist*
633 21, 173-480.
- 634 Hrouda, F. (2004) Problems in interpreting AMS parameters in diamagnetic rocks. In: F.
635 Martín-Hernández, C.M. Lueneburg, C. Aubourg, and M. Jackson (eds) *Magnetic*
636 *Fabric: Methods and Applications*. The Geological Society Special Publications 238,
637 49-59.
- 638 Jelinek, V. (1981) Characterization of the magnetic fabric of rocks. *Tectonophysics* 79, T63-
639 T67.
- 640 Jelinek, V. (1984) On a mixed quadratic invariant of the magnetic susceptibility tensor.
641 *Journal of Geophysics - Zeitschrift Fur Geophysik* 56, 58-60.
- 642 Lagroix, F., and Borradaile, G.J. (2000) Magnetic fabric interpretation complicated by
643 inclusions in mafic silicates. *Tectonophysics* 325, 207-225.
- 644 Laugier, J., and Filhol, A. (1983). An interactive program for the interpretation and simulation
645 of Laue patterns. *Journal of Applied Crystallography* 16, 281-283.
- 646 Martín-Hernández, F., and Hirt, A.M. (2001) Separation of ferrimagnetic and paramagnetic
647 anisotropies using a high-field torsion magnetometer. *Tectonophysics* 337, 209-221.
- 648 Martín-Hernández, F., and Hirt, A.M. (2004) A method for the separation of paramagnetic,
649 ferrimagnetic and haematite magnetic subfabrics using high-field torque
650 magnetometry. *Geophysical Journal International* 157, 117-127.
- 651 Neumann, F.E. (1885) *Vorlesungen über die Theorie der Elastizität der festen Körper und des*
652 *Lichtäthers*. 374p. B.G. Teubner Verlag, Leipzig, Germany.
- 653 Nye, J.F. (1957) *Physical Properties of Crystals: Their Representation by Tensors and*
654 *Matrices*. 338p. Clarendon Press, Oxford, UK.
- 655 Oberti, R., Hawthorne, F.C., Cannillo, E., and Camara, F. (2007) Long-range order in
656 amphiboles. In: Keppler H., Smyth, J.R. (eds) *Reviews in Mineralogy and*
657 *Geochemistry* 67, 125-171.
- 658 Parks, G.A., and Akhtar, S. (1968) Magnetic moment of Fe²⁺ in paramagnetic minerals. *The*
659 *American Mineralogist* 53, 406-415.
- 660 Parry, G.R. (1971). *The magnetic anisotropy of some deformed rocks*. 218p. PhD thesis,
661 University of Birmingham, Birmingham, UK.
- 662 Pettke, T., Oberli, F., Audetat, A., Guillong, M., Simon, A., Hanley, J., and Klemm, L.M.
663 (2012) Recent developments in element concentration and isotope ratio analysis of
664 individual fluid inclusions by laser ablation single and multiple collector ICP-MS. *Ore*
665 *Geology Reviews* 44, 10-38.
- 666 Reusser, C.E. (1987) *Phasenbeziehungen im Tonalit der Bergeller Intrusion*. PhD thesis,
667 Department of Earth Sciences. ETH Zurich, Zurich, Switzerland.
- 668 Schmidt, V., Hirt, A.M., Hametner, K., and Gunther, D. (2007a) Magnetic anisotropy of
669 carbonate minerals at room temperature and 77 K. *American Mineralogist* 92, 1673-
670 1684.
- 671 Schmidt, V., Hirt, A.M., Rosselli, P., and Martín-Hernández, F. (2007b) Separation of
672 diamagnetic and paramagnetic anisotropy by high-field, low-temperature torque
673 measurements. *Geophysical Journal International* 168, 40-47.
- 674 Schulmann, K., and Ježek, J. (2011) Some remarks on fabric overprints and constrictional
675 AMS fabrics in igneous rocks. *International Journal of Earth Sciences* 101, 705-714.

- 676 Spandler, C., Pettke, T., and Rubatto, D. (2011) Internal and external fluid sources for
677 eclogite-facies veins in the Monviso Meta-ophiolite, Western Alps: Implications for
678 fluid flow in subduction zones. *Journal of Petrology* 52, 1207-1236.
- 679 Vernon, R.H. (1961) Magnetic susceptibility as a measure of total iron plus manganese in
680 some ferromagnesian silicate minerals. *The American Mineralogist* 46, 1141-1153.
- 681 Verwey, E.J.W. (1939) Electronic conduction of magnetite (Fe_3O_4) and its transition point at
682 low temperatures. *Nature* 144, 327-328.
- 683 Wagner, J.-J., Hedley, I.G., Steen, D., Tinkler, C., and Vuagnat, M. (1981) Magnetic
684 anisotropy and fabric of some progressively deformed ophiolitic gabbros. *Journal of*
685 *Geophysical Research* 86, 307-315.
- 686 Walz, F. (2002) The Verwey transition - a topical review. *Journal of Physics: Condensed*
687 *Matter* 14, R285-R340.
- 688 Zak, J., Verner, K., and Tycova, P. (2008) Multiple magmatic fabrics in plutons: an
689 overlooked tool for exploring interactions between magmatic processes and regional
690 deformation? *Geological Magazine* 145, 537-551.